

2021

Impact of pressure drop oscillations on surface temperature and critical heat flux during flow boiling in a microchannel

M.D. Clark

J.A. Weibel

S.V. Garimella

Follow this and additional works at: <https://docs.lib.purdue.edu/coolingpubs>

Clark, M.D.; Weibel, J.A.; and Garimella, S.V., "Impact of pressure drop oscillations on surface temperature and critical heat flux during flow boiling in a microchannel" (2021). *CTRC Research Publications*. Paper 382.

<http://dx.doi.org/10.1109/TCPMT.2021.3094767>

This document has been made available through Purdue e-Pubs, a service of the Purdue University Libraries. Please contact epubs@purdue.edu for additional information.

Impact of Pressure Drop Oscillations on Surface Temperature and Critical Heat Flux during Flow Boiling in a Microchannel

Matthew D. Clark, Justin A. Weibel, and Suresh V. Garimella

Abstract— Flow boiling in microchannel heat sinks is capable of providing the high-heat-flux dissipation required for thermal management of next-generation wide bandgap power electronics at low pumping power and uniform surface temperatures. One of the primary issues preventing implementation of these technologies is the presence of flow boiling instabilities, which may reduce the heat transfer performance. However, the effect of individual instabilities, such as the parallel channel instability or pressure drop oscillations, on the overall heat transfer coefficient and critical heat flux in microchannel heat sinks has not been fully quantified. The primary cause of these dynamic flow boiling instabilities is the interaction between the inertia of a two-phase mixture in a heated channel and sources of compressibility located upstream of the inlet. In order to isolate the effect of pressure drop oscillations on flow boiling heat transfer performance, experiments are performed in a single square microchannel cut into a copper heat sink, with a controlled level of upstream compressibility. The impact of pressure drop oscillations on the heat transfer coefficient and critical heat flux is characterized through analysis of both time-averaged steady-state data as well as high-frequency pressure signals synchronized with high-speed visualization. The dielectric working fluid HFE-7100 is used in all experiments with a saturation temperature of 60°C at the channel outlet pressure. The occurrence and effect of pressure drop oscillations in 20 mm long microchannels of three different channel widths (0.5, 0.75, and 1 mm) are related to mass flux, the degree of two-phase flow confinement, and the severity of pressure drop oscillations.

Index Terms—Compressibility, electronics cooling, flow boiling, flow instabilities, microchannels, two-phase heat transfer.

I. INTRODUCTION

Thermal dissipation requirements of next-generation power electronics, high-performance computing, and radar systems will far exceed the capabilities of conventional heat sink technologies [1]–[3]. Microscale flow boiling offers promising potential to meet the needs of these devices while maintaining low pumping power and temperature uniformity. Compared to other single-phase heat dissipation strategies, flow boiling also provides some of the highest heat transfer coefficients available. However, there are several complications inherent to the practical implementation of

pumped two-phase systems. One is the critical heat flux limit inherent to the boiling process. However, before critical heat flux is reached, another concern is the occurrence of flow instabilities that could have deleterious effects on the heat sink performance. The broadest classification of two-phase flow instabilities as distinguished by Bouré *et al.* [4] is between static and dynamic instabilities. Static instabilities result in a transition between steady-state conditions, or can have a periodic behavior of switching between multiple steady conditions. Dynamic instabilities cannot be characterized by steady-state principles alone and are caused by an interaction between the inertia of a two-phase mixture in a heated channel and a source of compressibility ([5], [6]). Two dynamic instabilities of great importance in microchannel heat sinks are parallel channel instabilities and pressure drop oscillations [7]. The former are a result of interaction between the two-phase mixture within two or more hydrodynamically coupled channels, while the latter result from interactions between the two-phase mixture in a single channel or heat sink and a source of compressibility upstream of the inlet [8].

Upstream compressibility can be present in a system in the form of trapped air, flexible components, or a large volume of subcooled liquid. As vapor bubbles nucleate, grow, and become confined within a heated channel and the vapor quality increases, the pressure drop across the channel also increases. If there is a source of compressibility upstream of the channel inlet, the system will dynamically respond to the changing demand curve, pressurizing the compressible volume and momentarily reducing mass flux into the channel. Once the pressure within the compressible volume is high enough to overcome the increase in channel pressure drop, the mass flux into the channel increases and this cycle continues periodically. In a single 500 μm -diameter glass microchannel, Kingston *et al.* [9] found the frequency of this pressure drop oscillation to be in the range of 10 – 30 Hz.

The nature of this pressure drop oscillation and other two-phase flow instabilities has been extensively investigated throughout the years and is highlighted in a number of reviews ([4], [10]–[15]). Much of this past work concerns macroscale boiling systems such as heat exchangers or nuclear reactors ([4], [5], [16]), though there is general agreement that two-phase flow instabilities are of particular concern in microscale systems where vapor confinement and bubble clogging is

This material is based upon work supported by Ford Motor Company through the University Research Program (URP).

M. D. Clark, J. A. Weibel, and Suresh V. Garimella are with Cooling Technologies Research Center, School of Mechanical Engineering, Purdue

University, 585 Purdue Mall, West Lafayette, IN 47907 USA (jaweibel@purdue.edu).

Suresh V. Garimella is also with The University of Vermont, Burlington, VT 05405 USA.

inherent [15]. Liu *et al.* [17] demonstrated that control of compressibility upstream of a microchannel inlet is critical to proper understanding of heat transfer behavior, pointing to the wide scatter of datasets and correlations describing otherwise similar systems. They controlled compressibility by varying the volume of gas in a buffer reservoir located upstream of the test section inlet and measured the pressure, temperature, and mass flux oscillations occurring in 0.9 and 2.0 mm diameter tubes with a total length of 610 mm (270 mm heated length). Without upstream compressibility, the heat transfer coefficient was found to depend on mass flux and not heat flux, whereas the opposite was observed for cases with sufficient upstream compressibility. The channel length as well as inlet and outlet geometries investigated in the study differ significantly from those typical of microchannel heat sinks. Studies presenting results on the impact of instabilities on heat transfer in such microchannel geometries are largely limited to multi-channel systems where the emphasis is on preventing instabilities from occurring. For example, Wang *et al.* [18], Szczukiewicz *et al.* [19], and Kandlikar *et al.* [20] all implemented inlet restrictors to suppress instabilities and compared flow oscillations and heat transfer with microchannels that did not include inlet restrictors. Generally, these studies concluded that the suppression of flow instabilities results in a reduction in channel wall temperature. However, due to the coupled nature of instabilities such as the parallel channel instability and pressure drop oscillation in multi-channel heat sinks, these studies do not isolate the effect of pressure drop oscillations alone.

This study investigates the impact of pressure drop oscillations on the flow boiling performance in a microchannel by considering a situation in which only this individual instability can occur. A multi-channel heat sink without inlet restrictions would allow the occurrence of both parallel channel instabilities and pressure drop oscillations. Only in a single channel can pressure drop oscillations be isolated and the impact on surface temperature and critical heat flux investigated. To this end, flow boiling experiments are performed in single microchannels of varying geometries cut into a copper heat sink. Testing under two conditions with and without an upstream compressible volume provides respective cases of flow subjected to pressure drop oscillations and a stable flow reference. By comparing the heat transfer performance between these cases, we gain an understanding of the impact of pressure drop oscillations on heat transfer in a microchannel.

II. EXPERIMENTAL METHODS

A. Flow Loop

The experimental two-phase flow facility, schematically illustrated in Fig. 1, is charged with the dielectric fluid HFE-7100 [21]. All tubing in the flow loop is rigid stainless steel. In the reservoir, submerged cartridge heaters are used to maintain the bulk working fluid at saturated conditions, while chilled-water Graham condensers attached to the top of the reservoir allow non-condensable gases dissolved in the liquid to escape. A magnetically coupled constant volumetric flow gear pump (GB-P23, Micropump) draws liquid from the bottom of the reservoir. In order to prevent cavitation within the pump, a liquid-to-air heat exchanger is used to reduce the liquid temperature prior to the pump inlet. The flowrate into the test

section is controlled by metering a portion of the flow from the pump back into the reservoir through a bypass line. The remaining liquid flow routed to the test section first passes through a 2 μm filter (Swagelok, SS-4TF-2) to remove particulates and an activated charcoal filter (Pall 12011) to remove organic materials. The mass flowrate is measured by a Coriolis mass flow meter (Micromotion CMF010M). A custom-built electrically heated liquid preheater raises the liquid temperature to the desired inlet subcooling before entering the test section.

Given that any of the components described above can provide a source of compressibility in the form of trapped air or flexible materials, the downstream portion of the flow loop including the test section must be isolated from these upstream components. An established method for suppressing flow instabilities caused by upstream compressibility is to throttle the flow using a pressure-drop element ([7], [18]–[20], [22]), which prevents pressure waves from traveling further upstream. To this end, the needle valve (Swagelok, SS-4MG-MH) labeled ‘system throttle’ in Fig. 1 is adjusted to maintain a system pressure of at least 90 kPa above the test section outlet pressure. The system pressure is measured (Omega, PX302-050GV) directly upstream of the system throttle valve. This pressure, which is consistent across all experiments, is approximately an order of magnitude greater than the nominal pressure drop across the test section. Initial tests showed that this pressure drop across the needle valve is sufficient to suppress instabilities caused by any compressibility upstream of the system throttle.

In order to then introduce a controlled amount of compressibility into the flow path between the system throttle valve and the test section, a ‘buffer volume’ attached to the fluid line, as labeled in Fig. 1, was custom fabricated from a graduated cylinder to include threaded connections on either end. The bottom end is adapted to an NPT fitting for integration into the fluid line, while the top end is fitted with a plug to seal the chamber. The total volume of the buffer is approximately 40 mL. The pressure is also measured at the junction connecting the buffer volume to the fluid line (Omega, PX302-030GV). For the experiments performed in this study, two cases are presented: (i) without upstream compressibility and (ii) with a

Fig. 1. Diagram of the flow loop including an inset 3D model of the test section and buffer volume located within the blue dashed outline of the flow loop and a photograph of the test section.

large degree of upstream compressibility. For case (i), the ball valve labeled ‘buffer cut-off’ in Fig. 1 is closed, preventing any interaction between the test section and the buffer volume. For case (ii), the plug at the top of the cylinder is removed and the cylinder is filled with liquid until 35 mL of air at atmospheric pressure remains. The plug is re-installed, and the buffer cut-off valve opened. To prevent air trapped in the buffer volume from dissolving into the working fluid, a hollow aluminum float ball is placed in the cylinder to reduce the air-liquid interface area. An additional needle valve, labeled ‘inlet valve’ in Fig. 1, is placed between the buffer volume and the test section. This valve remains completely open during all experiments presented in the current study. To minimize the chance of any unwanted source of compressibility between the system throttle and the microchannel inlet, care was taken to minimize the flow lengths between these components, including within the test section itself.

B. Test Section

The test section, shown in cross section in Fig. 2 and as an exploded assembly in Fig. 3 is designed to provide necessary measurements while minimizing the length of the flow path to the microchannel inlet. Heat input is provided by five 200W cartridge heaters (Watlow 2039-3259) inserted into a copper block with an overall length of 40 mm. Power to the cartridge heaters is supplied by a 600 W power supply (Sorensen, DLM 80-7.5). A total of eight thermocouples are embedded into the heater block above the cartridge heaters. Four thermocouples are placed at equal distances along the centerline of the block while two thermocouples are introduced on opposing sides. These thermocouple rakes are used as a secondary measure of heat flux into the heat sink (as a reference for comparison with measured electrical power input minus calibrated heat losses) and as a measure of the mean heater block temperature for heat loss calibration. The heater block is supported from below by a ceramic thermal insulator (Macor) and a vertical compressive force is provided by four screws seated in a PEEK fixture. The heat sink, also made of oxygen-free copper, is a separate component from the heater block, allowing ease of interchangeability. For this study, single square-cross-section channels with widths of 0.5, 0.75, and 1 mm are machined into the top of three separate heat sinks. These channel geometries correspond to confinement numbers of 1.72, 1.09, and 0.86, respectively, where the confinement number is calculated according to:

$$Co = \left[\frac{\sigma}{g(\rho_l - \rho_v)D_h^2} \right]^{0.5}$$

The surface tension, σ , liquid density, ρ_l , and vapor density, ρ_v , are calculated at the mean channel pressure. Each of these confinement numbers is larger than a value of 0.5, suggesting that confinement effects are expected to play a significant role [23].

Both the heat sinks and heater block have a square cross-section of 20 mm \times 20 mm, resulting in a flow length of 20 mm. A thermal interface material (TIM) is placed between the heater block and heat sink. The TIM (Laird Technologies, Tflex 700) was chosen because its effective thermal resistance is not

sensitive to the contact pressure beyond 70 kPa. Knowing the heat flux measured in the heater block, the channel surface temperature is extrapolated from three thermocouples embedded within the heat sink, each placed 2.5 mm below the top heat sink surface at the channel inlet, center, and outlet. In this way, the measurement of the channel surface temperature does not require estimation of the TIM thermal resistance. The heat sink is held in alignment with the surrounding PEEK carrier using stainless steel pins. The PEEK carrier includes taps for measuring inlet and outlet temperatures and pressures

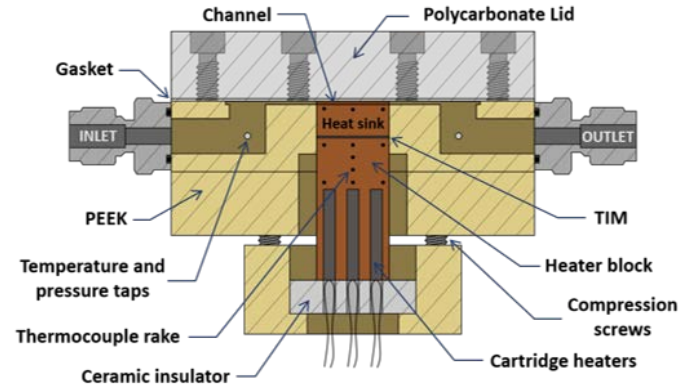


Fig. 2. Cross-sectional view of the test section with key parts and materials labeled.

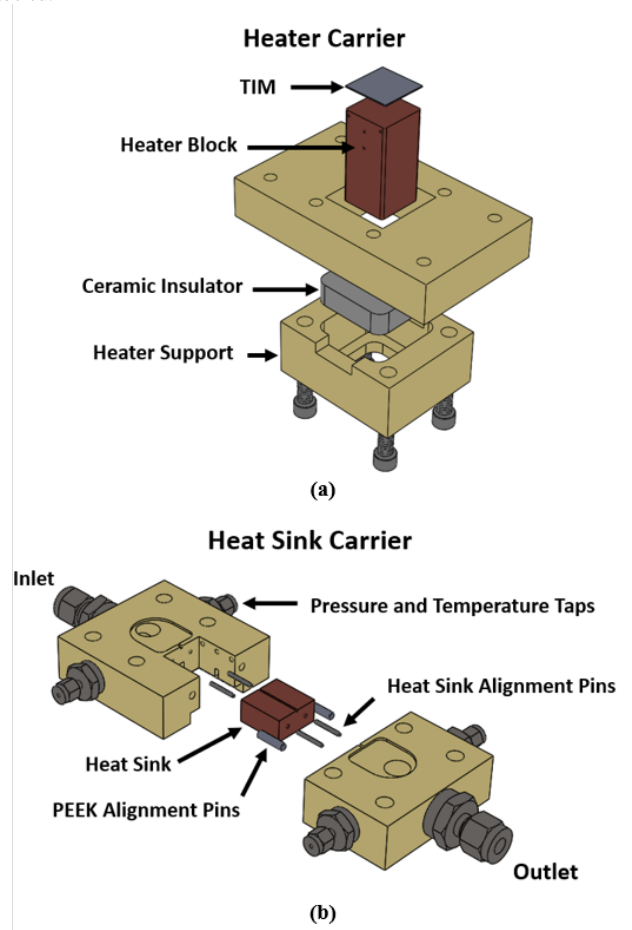


Fig. 3. Exploded assembly drawings of the (a) heater carrier and (b) heat sink carrier.

(Omega, PX302-030GV and PX302-030AV) in the respective plenums. The location of these measurement taps is shown in Fig. 2.

During assembly, sealant (Momentive, RTV118) is applied on all four sides of the PEEK carrier in contact with the copper heat sink. The top surfaces of the PEEK carrier and the heat sink are sealed using a transparent silicone gasket compressed between the top surfaces and a polycarbonate lid. To prevent the flexible silicone gasket from being squeezed into the channel and obstructing the flow, a thin intervening layer of PET is placed over the top surface of the copper heat sink.

C. Data Acquisition

All sensors are sampled using a data acquisition system (National Instruments cRIO-9024 with the necessary input/output modules). Resolving transient pressure fluctuations associated with pressure drop oscillations requires high-frequency characterization [24]. In this study, pressure transducers are sampled at a rate of 25 kHz. This signal is down-sampled to 2.5 kHz by averaging every 10 data points to reduce noise. All other data are sampled at a rate of 10 Hz and time-averaged at steady state. The temperature of the zero-point calibration reference (FLUKE, 9101) is measured using an RTD. Pressure transducer calibrations (Scandura, Pascal 100) and thermocouple calibrations (Isotech, Jupiter 4852) were performed prior to experimentation. Flow visualizations are acquired using a high-speed camera (Vision Research, Phantom v1212) paired with a 200 mm telephoto macro lens (Nikon, AF Micro-NIKKOR 200mm f/4D IF-ED). Both the high-frequency pressure signal sampling and high-speed videos are triggered simultaneously by the data acquisition system.

D. Experimental Procedure

Experiments are performed using three microchannel sizes (approximately 0.5, 0.75, and 1 mm) of square cross section and 20 mm flow length across a range of mass fluxes both with and without upstream compressibility. The actual channel dimensions, listed in Table I, were measured under a microscope (Olympus BX53M) and differ slightly from the nominal dimensions. Table II lists flowrates tested for each channel geometry. Prior to the start of an experiment, the working fluid is thoroughly degassed by vigorously boiling liquid in the reservoir while allowing non-condensable gases to escape through the Graham condensers and circulating fluid through the system for a minimum of 2 hr. Additionally, saturated boiling conditions are maintained in the reservoir throughout the experiment to ensure degassed conditions are held. At the beginning of an experiment, the channel mass flux, inlet subcooling, and buffer volume conditions are set while maintaining a system pressure of 90 kPa above the outlet pressure. In all experiments, the inlet subcooling is set to 20 °C as measured by the thermocouple at the test section inlet. Once these conditions are set, each experiment begins at zero power input to the heater block. Heater power is incremented in small steps, allowing steady-state conditions to be reached at each step, to produce a complete boiling curve including single-phase operation, nucleate boiling, and CHF conditions. Two datasets are acquired at steady state for each power increment: pressure signals are recorded at 25 kHz over 4 s and all other data are recorded at 10 Hz and time-averaged over a 2 min

TABLE I
MEASURED CHANNEL DIMENSIONS

Channel Width, w_c (μm)	Channel Height, h_c (μm)
508	530
788	756
1040	976

TABLE II
NOMINAL TEST PARAMETERS

Channel Width, w_c (mm)	Mass Flux, G ($\text{kg}/\text{m}^2\text{s}$)	Flow Rate, \dot{V} (mL/min)
0.5	400	4.1
	1000	10.1
	1600	16.2
	2000	20.3
0.75	100	2.3
	400	9.1
	1600	36.5
	2000	45.6
1	100	4.1
	400	16.2
	1600	64.9

period. High-speed videos are also acquired synchronized with the high-speed pressure measurement. This procedure is repeated to produce boiling curves by incrementing power from zero to CHF for cases (i) without and (ii) with an upstream compressible volume.

E. Data Reduction and Uncertainty Analysis

To measure heat loss from the heater block, Q_{loss} , a calibration experiment is performed with the heat sink removed and replaced with fiberglass insulation. Power is supplied to the heater block incrementally until the steady state temperatures measured within the heater block reach the maximum temperatures observed during the flow boiling experiments, providing the calibrated heat loss as a function of heater temperature. Heat flux within the heater block is calculated by subtracting Q_{loss} from the total electric power, P_{elec} , supplied to the cartridge heaters. The total electrical power supplied to the cartridge heaters is calculated from the voltage drop across the power supply and the electrical current measured using a 0.2 m Ω shunt resistor. This heat flux can also be calculated from a linear least-squares fit to the temperature gradient measured along the three thermocouple rakes within the heater block and the copper thermal conductivity (390 W/mK) according to Fourier's law. The difference in these two calculated values is small, indicating low heat losses.

Power input to the heat sink base is assumed equal to the power supplied to the heater block, and the channel wetted area heat flux is calculated according to the heat-loss-corrected power input divided by the area of the three exposed copper walls of each channel ($q'' = (P_{elec} - Q_{loss}) / A_{wet}$). Channel surface temperatures are extrapolated from the three thermocouples embedded 2.5 mm below the top surface of the heat sink to the bottom channel wall using the channel wetted area heat flux. When boiling occurs in the microchannels, the difference in surface temperatures extrapolated from the three

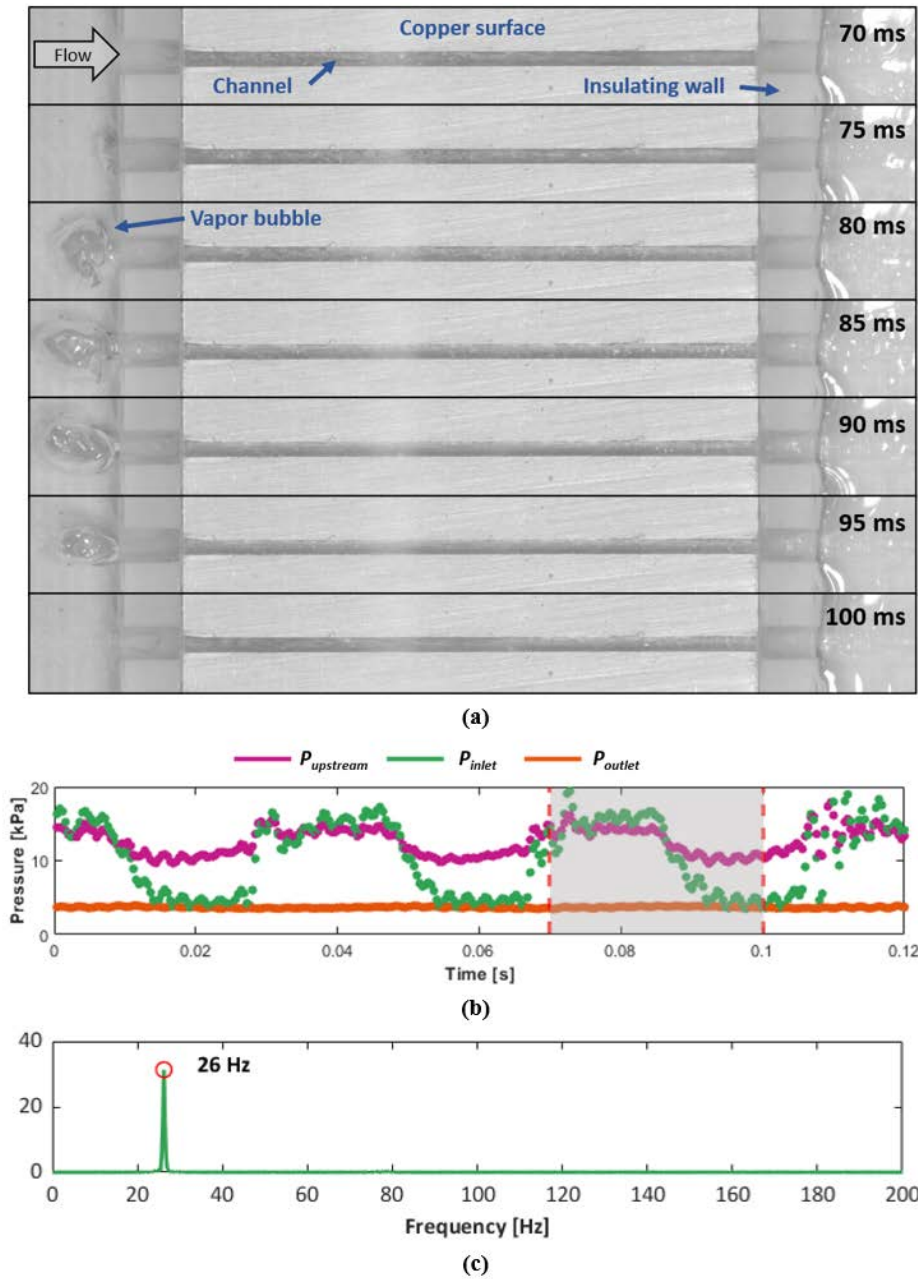


Fig. 4. (a) Visualization of a single backflow event ($w_c = 0.5$ mm, $G = 400$ kg/m²s, and $q'' = 25$ W/cm²), (b) synchronized pressure signal data, and (c) spectral power density of the P_{inlet} signal. The grey highlighted region of the pressure drop data corresponds to the period over which the video frames were captured.

heat sink thermocouples is negligible due to the high copper thermal conductivity and uniform heat transfer coefficient on the channel wall provided by nucleate boiling. Channel surface superheat is calculated as the difference between the average of the three extrapolated surface temperatures and the saturation temperature of HFE-7100 at atmospheric pressure as maintained in the reservoir.

During thermocouple calibration, the temperature of the dry-block calibrator is measured using an RTD with uncertainty of ± 0.15 °C. The ice-point reference temperature uncertainty is ± 0.02 °C. For each thermocouple, a linear offset from the standard NIST T-type conversion curve is fitted to the

calibration data. Based on a linear regression uncertainty analysis [25], the calibrated thermocouple uncertainty is estimated to be ± 0.3 °C. Pressure measurement uncertainty, calculated as the root sum of squares of the manufacturer-quoted errors, is estimated to be ± 2.13 kPa. From the manufacturer-quoted uncertainties of the equipment used to measure electrical power input and uncertainty in the channel geometry measurements, the calculated wetted area heat flux uncertainty ranges from approximately ± 0.1 W/cm² at the lowest heat fluxes to ± 1.2 W/cm² at the highest heat fluxes. Considering uncertainties in heat flux, thermocouple measurements, and thermocouple positions, the maximum uncertainty in the extrapolated channel surface temperature is estimated to be ± 0.4 °C.

III. RESULTS AND DISCUSSION

A. Identification of the Occurrence of Pressure Drop Oscillations

Before presenting and interpreting the complete set of data in the following sections, we first describe a single representative case alongside the methods used to determine the occurrence and severity of pressure drop oscillations within the microchannel. Across all experiments, the clearest evidence of pressure drop oscillations is the detection of backflow of vapor from the channel into the inlet header. This phenomenon has been observed by many researchers and was documented in the first reports of dynamic instabilities within microchannel heat sinks ([8], [9],

[26], [27]). A representative example of a single backflow event is shown in Fig. 4 using frames taken from the high-speed video spaced at 5 ms increments. This event is occurring in a 0.5 mm microchannel at a mass flux of $G = 400$ kg/m²s and channel wetted-area heat flux of $q'' = 25$ W/cm². The transient pressures $P_{upstream}$, P_{inlet} , and P_{outlet} are shown in a panel below the video frames. In this panel, the time range corresponding to the video frames shown above is shaded gray. The first video frame at 70 ms corresponds to the initial spike in pressure drop across the microchannel caused by vapor bubble confinement and growth. In subsequent frames from 75 – 85 ms, vapor within

the microchannel moves upstream, opposite the nominal flow direction (from left to right), flowing from the microchannel inlet and into the inlet header where a bubble can be clearly observed. During this period in the corresponding transient pressure signals, P_{inlet} rises above $P_{upstream}$, a strong indication of flow reversal. Once the compressible volume within the buffer upstream of the microchannel inlet is sufficiently pressurized to overcome the increase in channel pressure drop, the microchannel is flooded with subcooled fluid and any vapor remaining in the inlet header is either forced back into the channel or condensed by the incoming fluid as seen in the last frame at 100 ms. This process occurs cyclically resulting in the pressure oscillations seen in Fig. 4(b).

The spectral power density of the P_{inlet} signal is shown in Fig. 4(c). A clear peak occurs at 26 Hz corresponding to the frequency of the pressure drop oscillations. The appearance of a well-defined, singular frequency associated with the pressure drop oscillations, as revealed in this particular case, is representative of all cases where this instability occurs; otherwise, when the instability is not present, no dominant frequency is identified. For the experiments reported in the following section, the spectral power density is used to identify both the frequency and amplitude of the pressure oscillations.

B. Time-averaged Flow Boiling Behavior

Time-averaged steady-state boiling curves for each channel size and mass flux combination are presented in the plots on the left in Fig. 5. For each mass flux, (i) data points filled darker correspond to the tests without a compressible volume upstream of the heat sink inlet, while (ii) the lighter filling corresponds to tests run with a compressible volume. The boiling curves present the channel wetted-area heat flux plotted against the surface superheat, defined as the difference between the channel surface temperature and the saturation temperature of the fluid. The saturation temperature is calculated based on atmospheric pressure which is maintained in the reservoir connected to the outlet of the test section. To the right of the boiling curves in Fig. 5, the dominant frequency of the P_{inlet} signal and amplitude of oscillations are shown for all cases where backflow was observed as described in Section III.A. Oscillation amplitude is defined as $(P_{inlet,95} - P_{inlet,5}) / 2$, where $P_{inlet,95}$ and $P_{inlet,5}$ are the 95th and 5th

percentile of the inlet pressure data, respectively.

Each of the individual boiling curves follow a similar trend. At the lowest heat fluxes, the microchannel operates within the single-phase regime and the wall temperature increases linearly

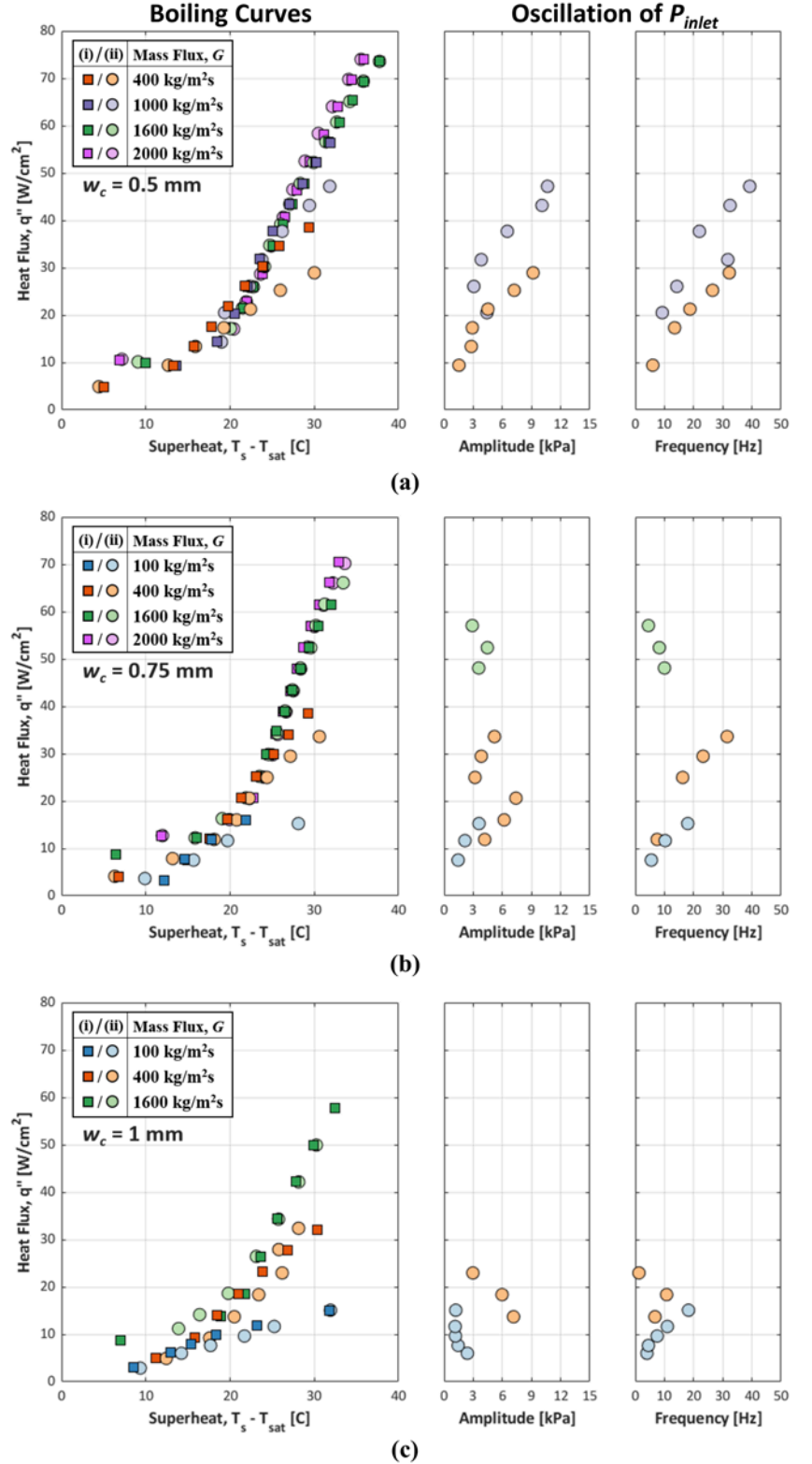


Fig. 5. Boiling curves (left) for cases (i) without and (ii) with an upstream compressible volume and dominant amplitude and frequency (right) in the P_{inlet} signal for all cases where backflow was observed for the three microchannel geometries: (a) 0.5 mm, (b) 0.75 mm, and (c) 1 mm.

with heat flux, as expected for internal convection with a constant heat transfer coefficient. Once nucleate boiling is initiated within the microchannel, the curve turns sharply upward in response to the increase in heat transfer coefficient. Generally, the data collapse within this regime indicating the heat transfer coefficient is independent of mass flux. Superheat excursion during boiling incipience is not observed in the current tests, though this does often occur with dielectric fluids ([28], [29]). Consequently, the explosive rapid-bubble-growth instability often observed at the onset of boiling incipience does not occur [24]. The microchannel operates within the nucleate boiling regime for a range of heat fluxes until critical heat flux is reached. While little variation in flow pattern during this range of heat fluxes is observed, under some conditions, the flow becomes annular very near to CHF. Generally, when CHF occurs at relatively low heat fluxes, the channel surface temperature is observed to gradually increase until the microchannel becomes filled with saturated vapor. In contrast, CHF at comparatively higher heat fluxes appears as a sharp increase in channel surface temperature and local dryout within the microchannel. For each individual boiling curve presented in Fig. 5, the data point at the highest heat flux corresponds to the last steady-state data recorded prior to the occurrence of CHF.

For a channel width of 0.5 mm (Fig. 5(a)) and the lower mass fluxes of 400 and 1000 kg/m²s, allowing the channel to interact with the buffer volume directly upstream results in a significant shift of the boiling curves to a higher surface superheat. As indicated by the appearance of a dominant amplitude and frequency in the P_{inlet} signal, the presence of a pressure drop oscillation is clearly identified to be responsible for this increase in temperature, given that the instability is isolated as the sole difference between the test cases (i) and (ii). Additionally, as heat flux increases, both the amplitude and frequency of the oscillations also increase. The magnitude of the increase in surface superheat also becomes more severe, increasing from 1.6 °C to 6 °C for the lowest mass flux of 400 kg/m²s. For both of these mass fluxes, a lower critical heat flux limit in the open buffer case (ii) having instabilities was also observed. The reduction in critical heat flux limit was 12. W/cm² for $G = 400$ kg/m²s and 10.2 W/cm² for $G = 1000$ kg/m²s. For the mass fluxes greater than 1000 kg/m²s, no difference between the open and closed buffer cases was observed, and the boiling curves collapse to the same trend. No backflow is observed in either of these cases, indicating the suppression of pressure drop oscillations when the flow inertia is sufficient large [9].

The observations made in the 0.75 mm channel are similar to those of the 0.5 mm channel. Namely, the presence of the compressible volume resulted in a shift of the boiling curve to higher surface superheats ranging from 0.5 °C to 6 °C for the lower 100 and 400 kg/m²s mass fluxes, which is attributed to the pressure drop oscillation. A small reduction in the critical heat flux limit of 4.6 W/cm² is observed at 400 kg/m²s with an open buffer, but there is no such effect observed for the lowest mass flux. However, we note that the reduction in critical heat flux for this 0.75 mm channel size is close to the magnitude of

the increments in steady-state power input, making the conclusion on the effect of the instabilities less conclusive compared to the notable increase in the surface superheat. Similar to the smaller 0.5 mm channel, the occurrence of backflow at higher mass fluxes is significantly reduced. Some low-amplitude intermittent pressure drop oscillations were observed at 1600 kg/m²s with an open buffer, but no impact on

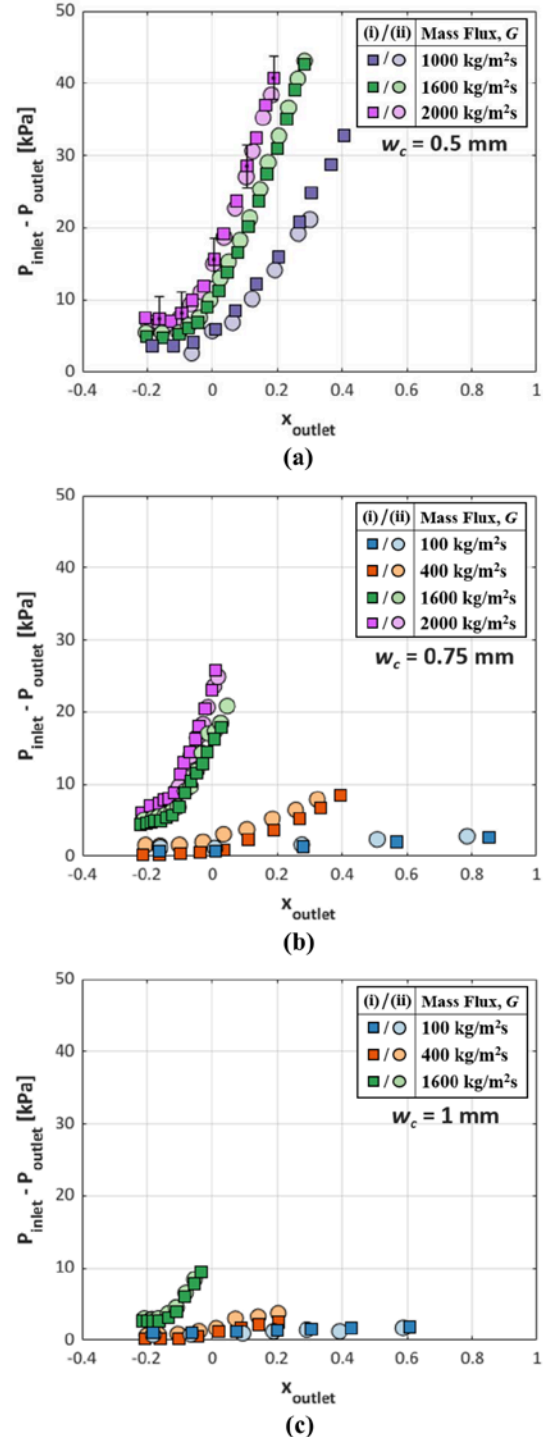


Fig. 6. Channel pressure drop, calculated as the difference between the inlet (P_{inlet}) and outlet (P_{outlet}) manifold pressures in the (a) 0.5 mm, (b) 0.75 mm, and (c) 1 mm microchannel geometries, plotted against the outlet vapor quality (x_{outlet}). Error bars showing uncertainty in calculated pressure drop are included for a representative data set at a mass flux of 2000 kg/m²s in the (a) 0.5 mm channel.

surface temperature was observed. No backflow was observed at the highest mass flux of 2000 kg/m²s.

In the largest channel size of 1 mm, backflow was observed at mass fluxes of 100 and 400 kg/m²s. For the lowest mass flux, backflow occurred at all heat fluxes where boiling was present in the channel and resulted in higher surface superheats of approximately 2 °C. Backflow was only observed at three steady-state heat fluxes at the intermediate mass flux of 400 kg/m²s. Before reaching critical heat flux, in this unique instance, the flow transitions to an annular regime, resulting in the suppression of pressure drop oscillations during the final two steady-state heat fluxes. Even for the cases where backflow was observed, the impact on surface temperature is minor compared to that observed in the smaller channel geometries, and there was no effect on the critical heat flux. These results indicate that this large channel is less susceptible to pressure drop oscillation, which is attributed to a lower degree of vapor confinement within the channel.

C. Time-averaged Channel Pressure Drop

Channel pressure drop is calculated as the difference between the inlet, P_{inlet} , and outlet, P_{outlet} , manifold pressures. Time-averaged steady-state pressure drop is plotted against outlet vapor quality in Fig. 6, where the outlet vapor quality is calculated according to:

$$x_{outlet} = \frac{h_{inlet} - h_f}{h_{fg}} + \frac{P_{elec} - Q_{loss}}{\dot{m} * h_{fg}}$$

The saturated liquid enthalpy, h_f , and the heat of vaporization, h_{fg} , are both evaluated at P_{outlet} .

For all of the mass fluxes, a characteristic response is observed: pressure drop is near constant during single-phase operation and increases with increasing outlet vapor quality due to vapor acceleration. The gradient of pressure drop with respect to vapor quality increases with increasing mass flux and decreasing channel width, as expected [13]. Increasing mass flux results in higher channel pressure drop for a given outlet vapor quality. At high mass fluxes, the flow is characterized by low vapor qualities, even at comparatively high heat fluxes, resulting in larger frictional pressure drop and smaller acceleration pressure drop. This is enhanced by the moderate inlet subcooling of 20 °C. Similarly, lower mass fluxes are characterized by high vapor qualities and the channel pressure drop is dominated by fluid acceleration due to vapor generation. Under similar inlet subcooling, Chen and Garimella [30] found that this balance of pressure drops due to friction and fluid acceleration resulted in channel pressure drop independent of mass flux for a given heat flux. There is little to no distinguishable difference in time-averaged channel pressure drop between the cases (i) with and (ii) without a compressible volume.

D. Influence of Severity of Instability on Surface Temperature

Mapping the relationship between the severity of pressure drop oscillations and the resulting impact on heat transfer performance is useful for understanding when this type of instability may become a concern in two-phase heat sink

design. Two quantifiable measures of the severity of pressure drop oscillations are the dominant frequency and amplitude of the oscillations. In the case of the current experiments, the pressure fluctuation signature is well represented by the inlet manifold pressure (P_{inlet}). The impact of pressure drop oscillations on flow boiling performance is represented by the difference in channel surface temperature between the open (T_{open}) and closed (T_{closed}) buffer cases. Fig. 7 shows both the

Fig. 7. Amplitude (left) and frequency (right) of the inlet manifold pressure (P_{inlet}) for all data points where backflow was observed in the (a) 0.5 mm, (b) 0.75 mm, and (c) 1 mm microchannel geometries, plotted against the temperature difference of the open and closed buffer configurations ($T_{open} - T_{closed}$).

amplitude and frequency of all cases where backflow was observed plotted against the surface temperature difference $T_{open} - T_{closed}$ between these two cases. Each of these data points corresponds to the data shown on the right panels of Fig. 5.

Pressure drop oscillation amplitudes range from 1 to 10 kPa and oscillation frequencies range from 5 to 40 Hz, which is in agreement with previous studies [9]. There is a clear trend of increasing surface temperature difference $T_{open} - T_{closed}$ for both increasing amplitude and frequency of the pressure drop oscillations in the smallest 0.5 mm microchannel. This trend is also clearly present with respect to oscillation frequency in the 0.75 mm microchannel. Both trends are less evident in the largest channel geometry, indicating a stronger dependence in smaller microchannels. This is attributed to reducing vapor confinement with increasing channel geometry. Across all three microchannel geometries, oscillations of amplitudes less than 4 kPa resulted in modest increases in surface temperature from 0 °C to 2 °C, while further increases in oscillation amplitude resulted in increases as high as 6 °C at an amplitude of 9 kPa.

Apart from the largest microchannel, the data show a positive relationship between the pressure drop oscillation frequency and temperature difference for individual channel sizes and flow rates. An exception to this trend is when pressure drop oscillations occur shortly after the onset of nucleate boiling. In one case corresponding to a mass flux of 1000 kg/m²s in the 0.5 mm channel, the pressure drop oscillations resulted in a greater area of activated nucleation sites within the microchannel and subsequent temperature decrease of 1.2 °C compared to the closed buffer case without oscillations. All other cases where pressure drop oscillations are observed resulted in either negligible difference or an increase in surface temperature.

The relationship between oscillation characteristics and temperature difference can be explained by the effect of flow reversal on the boiling process within the microchannel. During each backflow event, the microchannel is momentarily filled with vapor, disrupting the boiling process, and greatly reducing the transient heat transfer coefficient at the channel wall. With increasing amplitude and frequency of the pressure drop oscillations, we hypothesize that the total time over which the microchannel is filled with vapor, across many backflow cycles, increases. Consequently, this leads to decreasing time-averaged heat transfer coefficients and increasing channel wall temperature.

IV. CONCLUSIONS

Flow boiling experiments were performed in single square-cross-section microchannels of 0.5, 0.75, and 1 mm width over a range of mass fluxes (100 – 2000 kg/m²s) in a novel test section that allows characterization under controlled conditions without and with upstream compressibility. These two conditions allow for a comparison of stable flow and flow subjected to pressure drop oscillations, respectively. By comparing surface temperatures and critical heat flux data, the effect of pressure drop oscillations on heat transfer performance can be isolated and quantified, leading to the following primary conclusions:

- Control over interaction between the test section and sources of compressibility upstream of the inlet is

successfully demonstrated using a combination of an isolating system throttle valve and a buffer volume.

- The presence of a compressible volume upstream of a microchannel inlet is directly related to the occurrence of the pressure drop oscillation instability, which agrees with the established understanding.
- Pressure drop oscillation frequency (10 – 40 Hz) and amplitude (1 – 10 kPa) generally increase with increasing heat flux.
- For the microchannels tested, pressure drop oscillations lower critical heat flux limit in the smallest channel size of 0.5 mm, but have negligible effect on critical heat flux in larger microchannels.
- Pressure drop oscillations result in a reduction of heat transfer coefficient and increase in surface temperature. The degree of temperature rise attributable to the instability, ranging from 0.5 °C to 6 °C, increases with both amplitude and frequency of the pressure drop oscillation with a stronger dependence in smaller microchannel geometries.

ACKNOWLEDGMENT

Special thanks to Dr. Edward Jih at Ford Research & Advanced Engineering (R&AE) for technical discussions related to this work, and to Purdue undergraduate researcher Trevor Teague for his help performing the experiments presented in this work.

REFERENCES

- [1] A. Bar-Cohen, M. Arik, and M. Ohadi, "Direct liquid cooling of high flux micro and nano electronic components," *Proc. IEEE*, vol. 94, no. 8, pp. 1549–1570, Aug. 2006, DOI: 10.1109/JPROC.2006.879791.
- [2] K. P. Bloschok and A. Bar-Cohen, "Advanced thermal management technologies for defense electronics," in *Proc. SPIE 8405, Defense Transformation and Net-Centric Systems 2012*, May 2012, vol. 8405, p. 84050I, DOI: 10.1117/12.924349.
- [3] A. Bar-Cohen, J. J. Maurer, and J. G. Felbringer, "DARPA's Intra/Interchip Enhanced Cooling (ICECool) Program," in *CS MANTECH Conf.*, New Orleans, LA, USA, 2013, pp. 171–174.
- [4] J. A. Boure, A. E. Bergles, and L. S. Tong, "Review of two-phase flow instability," *Nucl. Eng. Des.*, vol. 25, no. 2, pp. 165–192, Jul. 1973, DOI: 10.1016/0029-5493(73)90043-5.
- [5] S. Kakac and B. Bon, "A Review of two-phase flow dynamic instabilities in tube boiling systems," *Int. J. Heat Mass Transf.*, vol. 51, no. 3, pp. 399–433, Feb. 2008, DOI: 10.1016/j.ijheatmasstransfer.2007.09.026.
- [6] S. G. Kandlikar, *Handbook of Phase Change: Boiling and Condensation*. 1st ed., Boca Raton, FL, USA, CRC Press, 1999.
- [7] A. Koşar, C.-J. Kuo, and Y. Peles, "Suppression of boiling flow oscillations in parallel microchannels by inlet restrictors," *J. Heat Transf.*, vol. 128, no. 3, pp. 251–260, Mar. 2006, DOI: 10.1115/1.2150837.
- [8] W. Qu and I. Mudawar, "Measurement and correlation of critical heat flux in two-phase micro-channel heat sinks," *Int. J. Heat Mass Transf.*, vol. 47, no. 10, pp. 2045–2059, May 2004, DOI: 10.1016/j.ijheatmasstransfer.2003.12.006.
- [9] T. A. Kingston, J. A. Weibel, and S. V. Garimella, "High-frequency thermal-fluidic characterization of dynamic microchannel flow boiling instabilities: Part 2 – Impact of operating conditions on instability type and severity," *Int. J. Multiph. Flow*, May 2018, DOI: 10.1016/j.ijmultiphaseflow.2018.05.001.
- [10] A. E. Bergles and S. G. Kandlikar, "On the nature of critical heat flux in microchannels," *J. Heat Transf.*, vol. 127, no. 1, p. 101, 2005, DOI: 10.1115/1.1839587.

- [11] J. R. Thome, "State-of-the-art overview of boiling and two-phase flows in microchannels," *Heat Transf. Eng.*, vol. 27, no. 9, pp. 4–19, 2006, DOI: 10.1080/01457630600845481.
- [12] S. G. Kandlikar, "History, advances, and challenges in liquid flow and flow boiling heat transfer in microchannels: A critical review," *J. Heat Transf.*, vol. 134, no. 3, pp. 034001-1–034001-15, Mar. 2012, DOI: 10.1115/1.4005126.
- [13] C. B. Tiberiçá and G. Ribatski, "Flow boiling in micro-scale channels – Synthesized literature review," *Int. J. Refrig.*, vol. 36, no. 2, pp. 301–324, 2013, DOI: 10.1016/j.ijrefrig.2012.11.019.
- [14] L. C. Ruspini, C. P. Marcel, and A. Clause, "Two-phase flow instabilities: A review," *Int. J. Heat Mass Transf.*, vol. 71, pp. 521–548, 2014, DOI: 10.1016/j.ijheatmasstransfer.2013.12.047.
- [15] Y. K. Prajapati and P. Bhandari, "Flow boiling instabilities in microchannels and their promising solutions – A review," *Exp. Therm. Fluid Sci.*, vol. 88, pp. 576–593, 2017, DOI: 10.1016/j.expthermflusci.2017.07.014.
- [16] H. Yüncü, O. T. Yildirim, and S. Kakaç, "Two-phase flow instabilities in a horizontal single boiling channel," *Appl. Sci. Res.*, vol. 48, no. 1, pp. 83–104, Jan. 1991, DOI: 10.1007/BF01998667.
- [17] Y. Liu, D. F. Fletcher, and B. S. Haynes, "On the importance of upstream compressibility in microchannel boiling heat transfer," *Int. J. Heat Mass Transf.*, vol. 58, no. 1, pp. 503–512, 2013, DOI: 10.1016/j.ijheatmasstransfer.2012.11.068.
- [18] G. Wang, P. Cheng, and A. E. Bergles, "Effects of inlet/outlet configurations on flow boiling instability in parallel microchannels," *Int. J. Heat Mass Transf.*, vol. 51, no. 9, pp. 2267–2281, May 2008, DOI: 10.1016/j.ijheatmasstransfer.2007.08.027.
- [19] S. Szczukiewicz, N. Borhani, and J. R. Thome, "Two-phase heat transfer and high-speed visualization of refrigerant flows in $100 \times 100 \mu\text{m}^2$ silicon multi-microchannels," *Int. J. Refrig.*, vol. 36, no. 2, pp. 402–413, Mar. 2013, DOI: 10.1016/j.ijrefrig.2012.11.014.
- [20] S. G. Kandlikar, W. K. Kuan, D. A. Willistein, and J. Borrelli, "Stabilization of flow boiling in microchannels using pressure drop elements and fabricated nucleation sites," *J. Heat Transf.*, vol. 128, no. 4, pp. 389–396, Dec. 2005, DOI: 10.1115/1.2165208.
- [21] 3M, 3M Novec Engineered Fluid HFE-7100 for Heat Transfer, 3M, St. Paul, MN, 2002, pp. 1–8.
- [22] A. Kaya, M. R. Özdemir, M. Keskinöz, and A. Koşar, "The effects of inlet restriction and tube size on boiling instabilities and detection of resulting premature critical heat flux in microtubes using data analysis," *Appl. Therm. Eng.*, vol. 65, no. 1, pp. 575–587, Apr. 2014, DOI: 10.1016/j.applthermaleng.2014.01.062.
- [23] P. A. Kew and K. Cornwell, "Correlations for the prediction of boiling heat transfer in small-diameter channels," *Appl. Therm. Eng.*, vol. 17, nos. 8–10, pp. 705–715, Aug. 1997, DOI: 10.1016/S1359-4311(96)00071-3.
- [24] T. A. Kingston, J. A. Weibel, and S. V. Garimella, "High-frequency thermal-fluidic characterization of dynamic microchannel flow boiling instabilities: Part 1 – Rapid-bubble-growth instability at the onset of boiling," *Int. J. Multiph. Flow*, vol. 106, pp. 179–188, Sep. 2018, DOI: 10.1016/j.ijmultiphaseflow.2018.05.007.
- [25] K. Brown, H. Coleman, and W. Steele, "Estimating uncertainty intervals for linear regression," in *Proc. 33rd Aerosp. Sci. Meet. and Exhib.*, Reno, NV, USA, 1995, DOI: 10.2514/6.1995-796.
- [26] D. Brutin, F. Topin, and L. Tadrist, "Experimental study of unsteady convective boiling in heated minichannels," *Int. J. Heat Mass Transf.*, vol. 46, no. 16, pp. 2957–2965, Jul. 2003, DOI: 10.1016/S0017-9310(03)00093-0.
- [27] H. Tuo and P. Hrnjak, "Periodical reverse flow and boiling fluctuations in a microchannel evaporator of an air-conditioning system," *Int. J. Refrig.*, vol. 36, no. 4, pp. 1263–1275, Jun. 2013, DOI: 10.1016/j.ijrefrig.2013.02.001.
- [28] A. Bar-Cohen and T. W. Simon, "Wall superheat excursions in the boiling incipience of dielectric fluids," *Heat Transf. Eng.*, vol. 9, no. 3, pp. 19–31, 1988, DOI: 10.1080/01457638808939668.
- [29] S. M. You, A. Bar-Cohen, and T. W. Simon, "Boiling incipience and nucleate boiling heat transfer of highly wetting dielectric fluids from electronic materials," *IEEE Trans. Compon. Hybrids Manuf. Technol.*, vol. 13, no. 4, pp. 1032–1039, 1990, DOI: 10.1109/33.62545.
- [30] T. Chen and S. V. Garimella, "Measurements and high-speed visualizations of flow boiling of a dielectric fluid in a silicon microchannel heat sink," *Int. J. Multiph. Flow.*, vol. 32, pp. 957–971, 2006, DOI: 10.1016/j.ijmultiphaseflow.2006.03.002.